Automated Load–Settlement Prediction of Shallow Foundations from Pushed-in PENCEL Pressuremeter Data Based on Briaud (2007) Method: A Python-Based Framework

Brhane W. Ygzaw[1*], PhD., Paul J. Cosentino, Ph.D., P.E.[1]
[1]Department of Mechanical and Civil Engineering, Florida Institute of Technology, Melbourne, FL 32901
[*]Corresponding author, Email: bygzaw2022@my.fit.edu
This version is a preprint and is currently under review at a peer-reviewed journal.

Abstract

This study presents a fully automated, Python-based framework for predicting shallow foundation settlements from pushed-in PENCEL pressuremeter (PPMT) data, using an adapted implementation of Briaud's (2007) method. The framework transforms raw in-situ test results into design-grade load–settlement curves by automating key analytical steps, including borehole wall-point detection, Lemée-type extrapolation for incomplete curves, strain-specific pressure extraction, and Schmertmann-based strain influence zoning. Unlike traditional approaches, which often rely on manual interpretation or pre-bored pressuremeter data, this method extends Briaud's framework to pushed-in PPMT devices, which offer logistical advantages in sandy soils. Correction factors for footing shape, load eccentricity, inclination, and slope proximity are included to reflect real-world boundary conditions. The framework's predictions were validated against advanced PLAXIS 3D simulations and full-scale field measurements across three Florida sites, demonstrating close agreement and confirming its reliability in cohesionless soils. By automating a traditionally complex procedure and supporting open-source reproducibility, this tool enables faster, more consistent deformation-based foundation design. The framework, implemented in Python, has been validated using field data and simulations and is publicly available for geotechnical practice and research.

Key words: Pressuremeter Test, Shallow Foundation Settlement, Briaud's Method, Python-Based Automation, PENCEL Pressuremeter, Load–Settlement Curve, Cohesionless Soils

Graphical Abstract

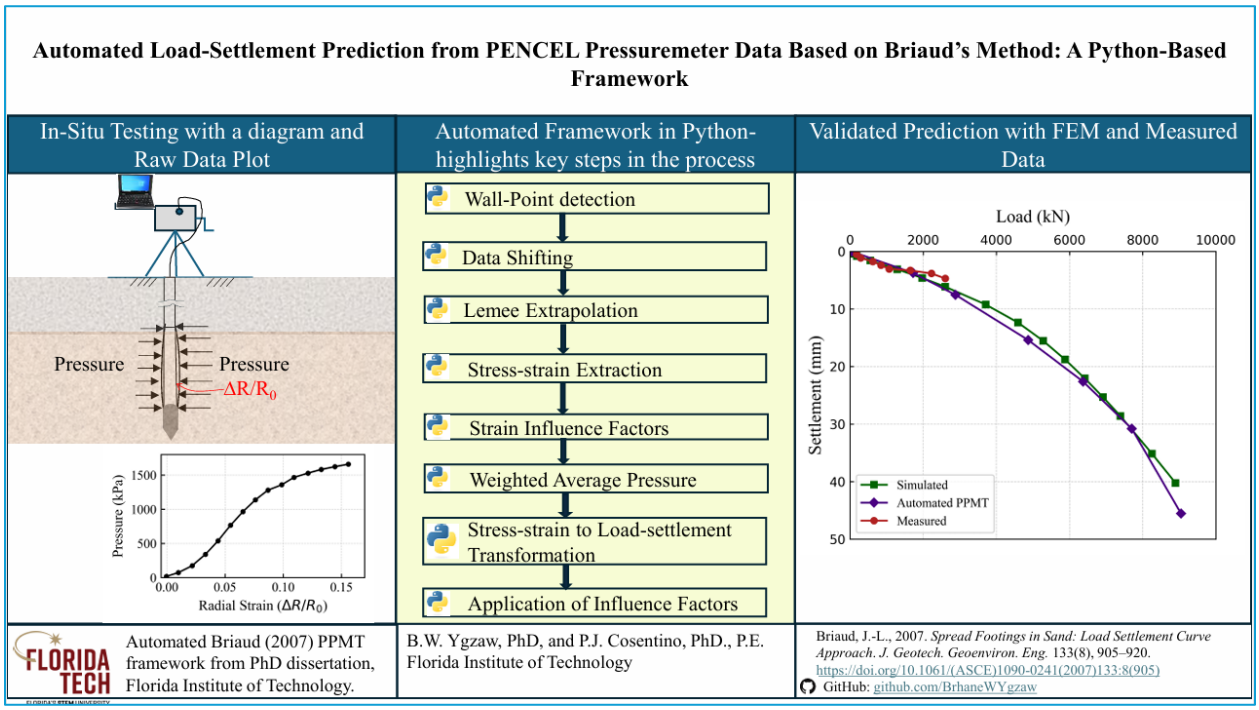

1. Introduction

Accurate prediction of settlement under shallow foundations remains a fundamental challenge in geotechnical engineering, particularly in granular soils where stiffness is highly nonlinear and stress-dependent. While a range of empirical and analytical methods are available–many based on in-situ tests such as the Standard Penetration Test (SPT), Cone Penetration Test (CPT), and flat dilatometer test (DMT)–these approaches rely heavily on empirical correlations and often fail to capture the actual deformation behavior of soils at working strain levels. Numerical simulations and artificial intelligence (AI)-based models offer alternative pathways but require high-quality input parameters or extensive training datasets, and often lack transparency in their predictions.

In contrast, the pressuremeter test (PMT) provides direct access to the nonlinear stress–strain behavior of soil in situ, making it a compelling basis for settlement prediction. Among the available PMT-based methods, Briaud (2007) proposed one of the most comprehensive procedures, combining in-situ stress–strain data with Schmertmann-type strain influence zoning and correction factors for boundary conditions such as footing shape and load eccentricity. However, the method was developed primarily for pre-bored pressuremeters and remains largely manual in its application. No open-source computational tool currently implements this method fully, and to the authors' knowledge, no published study has directly validated its predictions against both numerical simulations and full-scale field measurements, particularly in the context of pushed-in pressuremeter data.

To identify which settlement prediction approach offers the most consistent performance in practice, this study first conducts a comparative evaluation of shallow foundation settlement estimates using five in-situ test types–SPT, CPT, DMT, seismic CPT, and pushed-in PENCEL PMT (PPMT)–across three well-instrumented sites in Florida. The results indicate that the Briaud (2007) method, when applied to PPMT data, yields more consistent and physically realistic settlements than other in-situ and empirical approaches. This is particularly significant in cohesionless soils, where the PPMT offers the dual advantages of reduced disturbance and high data resolution.

These findings motivate the primary objective of this study: to develop a fully automated, Python-based framework for implementing Briaud's method using pushed-in pressuremeter data. The framework addresses the method's complexity and manual nature by incorporating automated modules for borehole wall-point detection, Lemée-type-curve extrapolation, depth-weighted pressure averaging, and foundation correction factor integration. It extends Briaud's original formulation to support modern PPMT devices and offers practical design outputs in the form of continuous load–settlement curves.

To validate the reliability of the automated approach, settlement predictions are compared against advanced finite element simulations (PLAXIS 3D) and full-scale field measurements from the three selected sites. Results show strong agreement across cases, confirming that the automated PPMT-based method offers both technical rigor and field applicability.

By automating a robust but underused analytical procedure and demonstrating its value through comparative evaluation and field validation, this work contributes both a novel computational tool and evidence supporting broader adoption of PPMT-based settlement design in granular soils. The open-source nature of the framework further enhances its potential as a scalable, transparent, and reproducible solution for modern geotechnical practice.

2. Background

Shallow foundation design in granular soils is often governed by settlement performance rather than bearing capacity. Predicting this settlement with confidence requires accurate characterization of stress-dependent soil stiffness, something that many traditional design approaches struggle to achieve. Over the years, a range of analytical, empirical, and computational methods have been proposed, each with varying trade-offs in accuracy, complexity, and generality.

Analytical methods based on classical elasticity, such as Schleicher's early solutions (Schleicher, 1926) and the formulations by Poulos and Davis (1974), estimate settlement under the assumption of linear-elastic, homogeneous soil. Mayne and Poulos (1999) extended these models to account for depth-dependent stiffness, improving their realism in layered soils. While theoretically elegant, these models often fall short in representing nonlinear behavior and localized soil-structure interaction.

Terzaghi's one-dimensional theory and its operationalization by researchers such as Webb, (1970) and Oweis (1979) remain foundational for consolidation-induced settlement in cohesive soils. However, the assumptions of isotropy, homogeneity, and linearity limit the accuracy of these approaches in real-world, heterogeneous conditions.

To address these limitations, empirical and semi-empirical methods have emerged, particularly those based on in-situ testing. Schmertmann's CPT-based strain influence method (Schmertmann, 1970; Schmertmann, 1978) remains widely used, and additional CPT-based stiffness correlations have been developed by Meyerhof (1965), Papadopoulos (1992), and De Beer and Martens (1957). SPT-based settlement estimations by Hough (1959), Terzaghi and Peck (1968), and Bowles (1996) offer practical alternatives, though they are sensitive to energy variability and stratigraphic irregularities.

Pressuremeter-based approaches have emerged as a compelling alternative for capturing in-situ stress–strain behavior. Ménard and Rousseau (1962) laid the foundation, and Briaud (2007, 1992) expanded on this with a comprehensive settlement prediction method that incorporates strain influence profiles and correction factors for foundation geometry, load eccentricity, and ground slope. Despite their strengths, most PMT-based methods were developed using pre-bored devices, and interpretation typically requires significant manual effort.

DMT tests have also been used for deformation-based settlement predictions based on some commonly used approaches (Leonards and Frost, 1988; Schmertmann, 1986). They offer quick stiffness profiling, but require site-specific calibration for reliable results.

Numerical simulations, especially those using FEM, FDM, or BEM, enable detailed modeling of layered, nonlinear, and time-dependent soil behavior. Jin et al. (2019) showed that incorporating PMT-based moduli into FEM models improves predictive accuracy. However, these methods require high-quality input data and are sensitive to constitutive assumptions and boundary conditions.

In parallel, machine learning approaches have gained attention for their potential to model complex relationships using data-driven techniques. Studies by Bagińska and Srokosz (2019), Liu and Liang (2024), and Marto et al. (2014) have used neural networks, ensemble learning, and hybrid models to predict bearing capacity. Aouadj and Bouafia (2022), Mohanty and Das (2018), extended these models to settlement prediction. While these methods often achieve strong statistical performance, they remain black-box models and typically lack transparency and generalizability across sites.

Among all these methods, Briaud (2007) PMT approach stands out as one of the most comprehensive and mechanistically grounded. It integrates in-situ nonlinear stress–strain data with Schmertmann-type strain influence zoning and correction factors for real-world foundation conditions. The method was designed primarily for pre-bored pressuremeters and involves multiple manual steps such as wall-point detection, spatial averaging, and correction factor application.

However, Briaud's method has not been systematically validated or adapted for use with pushed-in pressuremeters, such as the PENCEL PPMT, which offer logistical and technical advantages in sandy soils. These include reduced disturbance, faster deployment, and improved profiling resolution. Moreover, the method lacks a formal procedure for extrapolating incomplete stress–strain curves, a common issue in practice, especially with PPMT data that may not reach the limit pressure.

To address these limitations, this study develops a fully automated, Python-based framework implementing Briaud's method using pushed-in PPMT data. The framework introduces a Lemée-type extrapolation model (LEMÉE, 1973) for extending incomplete pressuremeter curves and automates all key stages from wall-point detection to pressure averaging and load–settlement curve generation. The results are validated against both finite element simulations (PLAXIS 3D) and full-scale field measurements at three instrumented Florida sites. These findings demonstrate that the adapted method is both effective and practical for use in cohesionless soils and that automation can unlock its broader adoption in modern geotechnical practice.

Key Contributions:

- First full automation of Briaud's (2007) method for PPMT.
- Validation with field, numerical, and experimental data.
- Open-source, reproducible framework tailored for granular soils.

3. Methodology

This study develops a fully automated Python-based framework to implement Briaud's (2007) method for predicting the load–settlement behavior of shallow foundations from pressuremeter data. The framework is designed to process raw PPMT input, identify the wall contact point, apply curve shifting and extrapolation (as needed), extract pressure values at specific strain levels, apply depth-based weighting and correction factors, and generate a complete footing load–settlement curve suitable for design.

The entire computational process is modular and sequenced to mirror the logic of the original Briaud method, with added enhancements for reproducibility and field adaptability. A high-level schematic of this automated workflow is provided in Fig. 1 illustrating how each functional block, from raw test input to final settlement prediction, is implemented in the code.

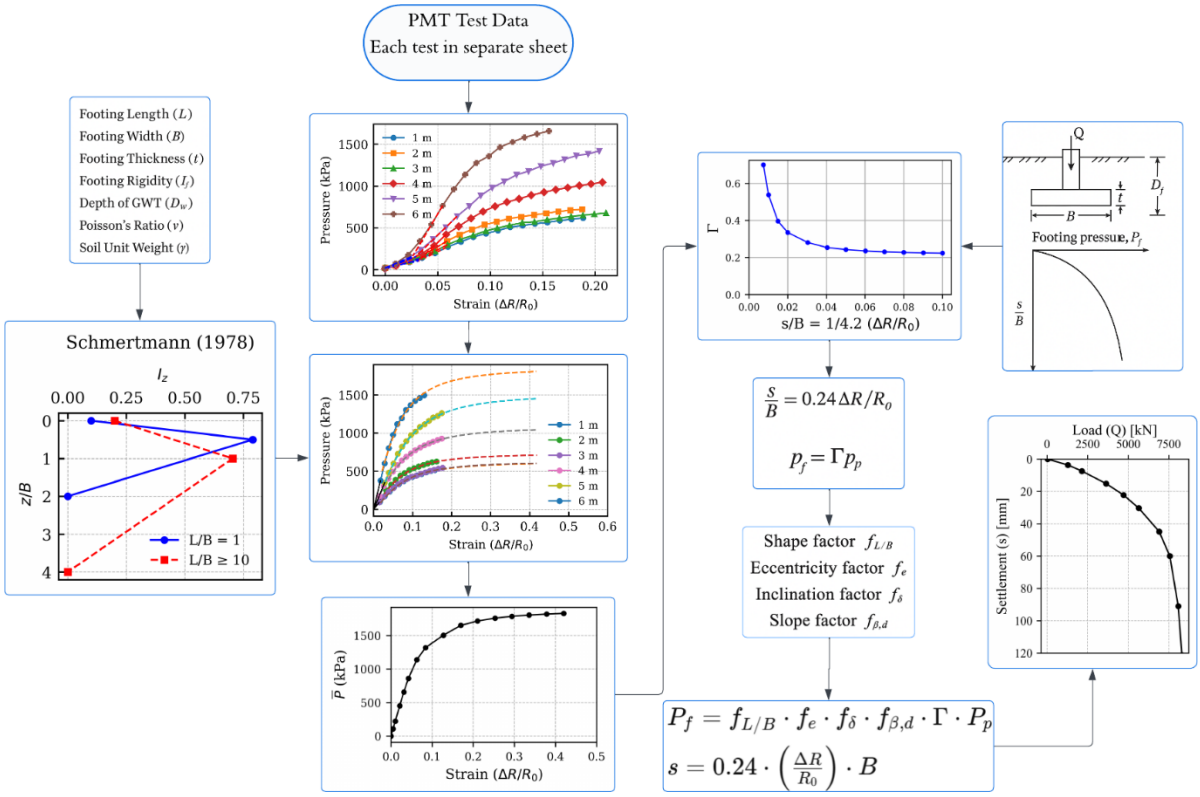

Fig. 1. A flowchart depicting the methodology followed in the load-settlement prediction approach

3.1. User Inputs and Test Data Structure

The framework begins with user-specified input values that define the foundation geometry and loading conditions provided in Table 1 and PMT data recorded at different depths.

Table 1. User-Specified inputs for the automated Briaud (2007) framework

Input description	Unit	Input description	Unit
Footing Dimensions		Applied load, Q	kN
Length, L	m	Unit weight, γ	kN/m^3
Width, B	m	Eccentricity	-
Thickness, t	m	Load inclination angle	(^{0})
Foundation depth, D_f	m	Distance to slope	m
Depth of groundwater table, D_w	m	Slope angle, H: V	-

Field test data are read from a multi-sheet Excel file, where each sheet corresponds to a specific depth's pressuremeter test. The framework dynamically identifies the header row and searches for two required columns: Radial Strain (ΔR/R₀) and Reduced Pressure (kPa), using flexible keyword matching.

3.2. Wall Point Detection

The first step in the framework is to identify the wall contact point, the location where the expanding pressuremeter membrane first hits the borehole wall. This point marks the beginning of soil deformation and serves as the new origin for interpreting pressure–strain relationships in the analysis. To identify this wall point programmatically, the algorithm fits two linear segments to the pressure–strain curve:

- **Line 1 (L_1):** A best-fit line through the initial data points before the probe contacts the borehole wall, corresponding to probe expansion in air or in the liftoff zone.
- **Line 2 (L_2):** A second line fit to the portion of the curve after the onset of contact, where the pressure–strain relationship stabilizes briefly into a more linear trend.

The intersection of these two lines is taken as the wall point. This method mirrors the approach shown in Fig. 2, which presents a sample stress–volume curve from a pushed-in PENCEL pressuremeter test, delineating key regions: lift-off, pseudo-elastic, elasto-plastic, and plastic. Once the wall point is determined, all subsequent strain (or volume) and pressure values are shifted to this point so that this point becomes the new origin ($\varepsilon = 0$).

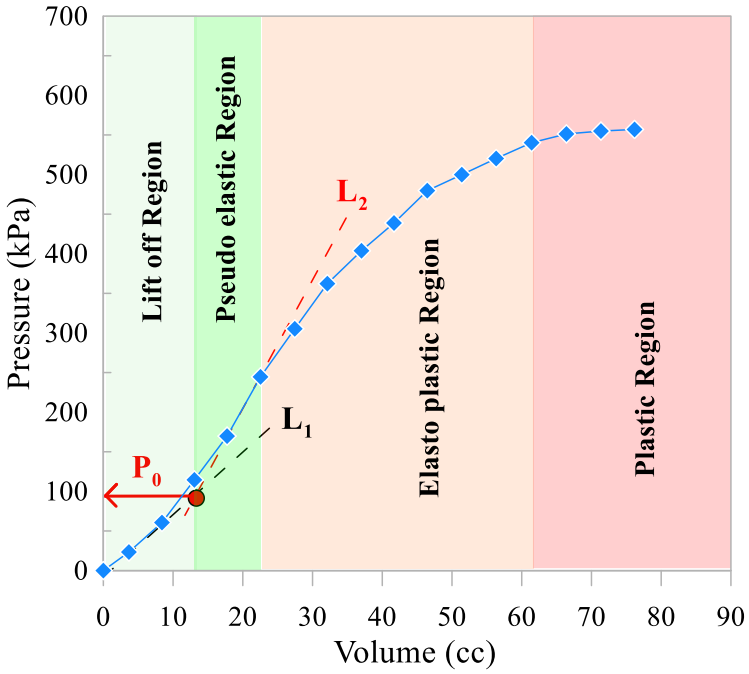

Fig. 2. Pressure–volume curve from PPMT showing contact pressure (P_0), pseudo-elastic region, and yielding.

3.3.Extrapolation to Limit Pressure

The loading phase of a PMT test is commonly halted before reaching the limit pressure. However, to ensure consistent settlement prediction using Briaud's (2007) method, the test data should be extrapolated up to a reference strain corresponding to the limit pressure, typically

associated with a cavity strain of 0.414 or a probe volume of $V_0 + 2Vc$ (Baguelin et al., 1978; Briaud, 2007) where: V_o is the initial probe volume, and V_c is the volume of water injected until the membrane first contacts the borehole wall.

Several extrapolation techniques are used in practice. The visual extrapolation is the simplest method, where data points are manually extended target strain or volume ($V_0 + 2V_c$). This is the simplest method, but subject to user interpretation. Others are the log-log method, upside-down curve method, relative volume method, and the Lemée method.

Fig. 3 illustrates the output of each method using the same PMT test data. While all techniques aim to identify the limit pressure, their estimates may vary depending on data quality and fitting assumptions.

In this study, the Lemée method was selected for implementation due to its stability, reproducibility, and ease of integration into code. However, the framework is modular and could accommodate alternative extrapolation strategies, if required.

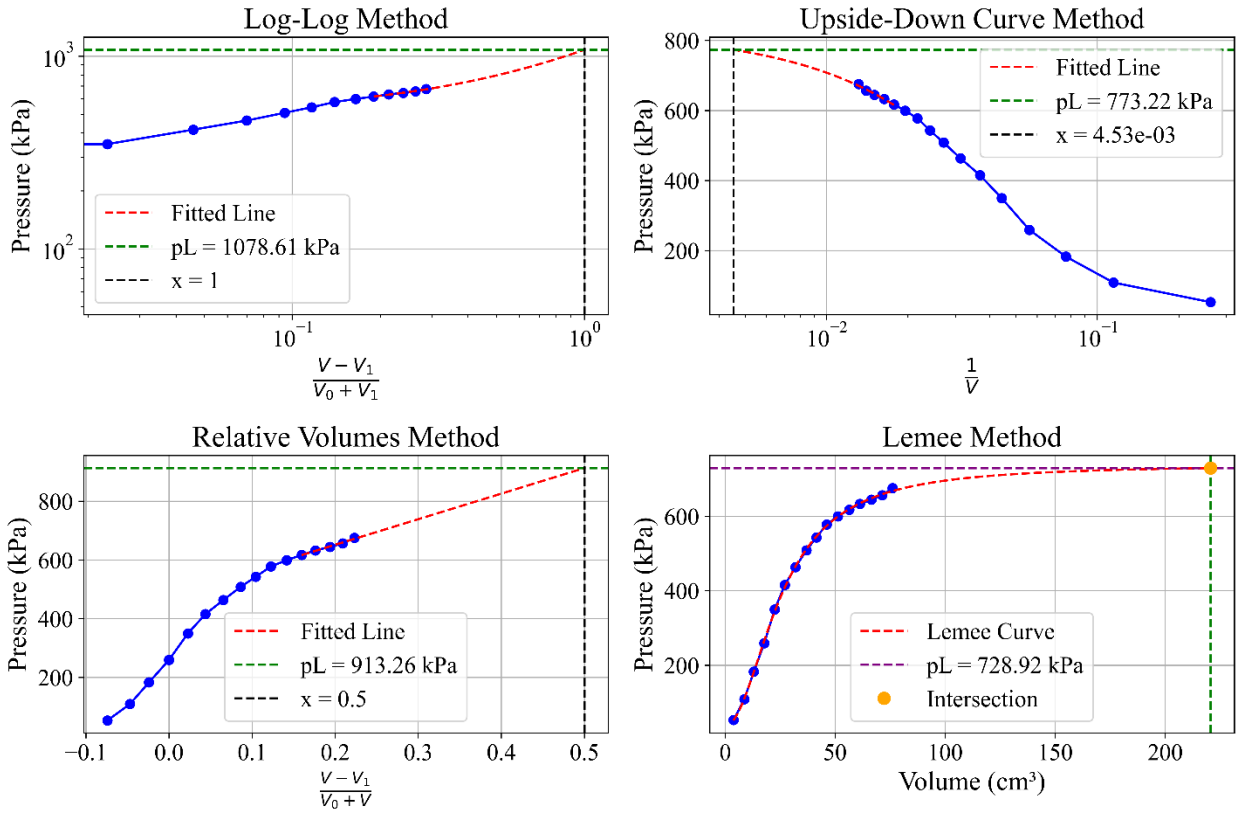

Fig. 3. The four different methods of prediction for the limit pressure (prepared based on (Baguelin et al., 1978))

3.4.Lemée-Type Curve Extrapolation

The approach employs a rational function to model the pressure–strain relationship beyond the measured data as given in Eq. (1).

$$P(\varepsilon) = \frac{b\varepsilon^2 + ac}{\varepsilon^2 + a} \tag{1}$$

where $\varepsilon = \Delta R/R_0$ is the radial strain, and a, b, and c are curve-fitting coefficients. The parameters a and b are derived from nonlinear regression using the final portion of the measured curve, while c is calculated to ensure that the extrapolated curve passes through the wall point (ε_0, P_0). This anchoring condition yields:

$$c = \frac{P_0\left(\varepsilon_0^2 + a\right) - b\varepsilon_0^2}{a} \tag{2}$$

This ensures the extrapolated segment maintains physical continuity with the observed data. The extrapolation is carried out from the wall point up to a maximum strain of $\varepsilon_{max} = 0.414 + \varepsilon_0$.

3.5. Pressure Extraction at Target Strain Levels

The pressure values of a certain borehole, at different depths, are arranged based on their strain levels. To simplify this procedure, target strain levels should be provided by the user and the pressure values at each test depth for those strain levels automatically collected by the automated framework. These strain levels should span the expected deformation range of the soil, extending up to $\varepsilon = 0.414$.

The framework employs a three-part logic to extract pressure values depending on the location of each ε_i relative to the available data:

- **(i) Pseudo-elastic Region:** For strain values between the wall contact point and the inflection where the stress–strain curve begins to bend, pressure is computed from the fitted Line 2 (L_2) using a linear expression:

$$P(\varepsilon) = P_0 + m(\varepsilon - \varepsilon_0) \tag{3}$$

  Where m is the slope of L_2.
- **(ii) End of linear portion to end of test data:** For this portion, pressure is obtained through direct linear interpolation. This is done based on the raw test data and avoids artificial distortions introduced by higher-order fits.
- **(iii) Extrapolated Region (Lemée Curve):** When ε_i exceeds the maximum observed strain, pressure is calculated using the Lemée extrapolation curve, calibrated to pass through the wall point and extend to $\varepsilon = 0.414$. This ensures smooth continuation of the curve beyond the data range.

By using region-specific logic, this method ensures accurate and physically meaningful pressure values across the full deformation spectrum, from initial probe contact to ultimate soil response.

For each test, the extracted pressure values are stored in structured arrays and passed to the subsequent module, which computes depth-weighted averages and generates the final load–settlement response.

3.6. Strain Influence Factor and Weighted Average Pressure Computation

To account for the depth-dependent contribution of soil layers to foundation settlement, this framework adopts the strain influence factor method proposed by Schmertmann (1978). The vertical distribution of strain beneath a footing varies based on the footing's shape and embedment, influencing how much each pressuremeter test contributes to the overall deformation. The framework discretizes the soil profile beneath the footing and assigns weights to each depth according to the empirical strain diagrams defined by Schmertmann.

Incorporating the strain influence factor allows the framework to realistically model how deformation varies with depth beneath the footing. This not only enhances the physical accuracy of the settlement prediction but also enables efficient and scalable integration of pressuremeter data across different test depths.

3.6.1. Dynamic Strain Area Weighting by Depth

Following the establishment of the vertical strain influence profile beneath the footing, the next step in the framework is to determine how much each pressuremeter test contributes to the overall settlement calculation. Since the pressuremeter tests are performed at discrete depths while the strain distribution is continuous, a numerical integration scheme is required to assign appropriate weight to each test. This is achieved through a dynamic strain area-based weighting method, where each test is associated with a region of the strain profile, and the area under this region defines its influence.

Let the total number of pressuremeter tests be n, each conducted at depth z_i, with i = 1, 2, …, n. The vertical domain of influence is bounded by the depth of the footing base D_f, at the top and the depth of zero strain, D_z, at the bottom. For each test, a segment of the depth domain is assigned, defined between the midpoints of the adjacent test depths, or between the domain boundaries for the first and last tests.

The area A_i associated with each test is computed by numerical integration of the strain profile over its assigned segment. When the strain function is approximated linearly within each segment, this reduces to the trapezoidal rule. For a test located between two segment boundaries at depths $z_{i-1/2}$ and $z_{i+1/2}$, the corresponding area is:

$$A_i = \frac{1}{2}\left[I_z\left(z_i - 1/2\right) + I_z\left(z_i + 1/2\right)\right] * \left[\left(z_i + 1/2\right) - \left(z_i - 1/2\right)\right] \tag{4}$$

Here, $I_z(z_{i-1/2})$ and $I_z(z_{i+1/2})$ are the strain values at the top and bottom of the segment, respectively, and are obtained by interpolation from the continuous profile. If the segment spans

the depth at which the strain reaches its maximum, it is split at that point, and two sub-areas are computed to maintain accuracy across the change in gradient.

Once all individual segment areas A_i are computed, the total area of influence is determined as:

$$A_{total} = \sum_{i=1}^{n} A_i \tag{5}$$

The normalized weight assigned to each test is then:

$$w_i = \frac{A_i}{A_{total}} \tag{6}$$

These weights reflect the relative contribution of each test to the deformation beneath the footing. Tests located near the peak of the strain profile, typically just beneath the footing base, are assigned higher weights, while those farther from the maximum zone are down-weighted accordingly.

3.6.2. Weighted Average Pressure Computation

With the normalized strain-based weights, w_i, assigned to each pressuremeter test, the framework proceeds to compute the depth-averaged pressure profile corresponding to each specified strain level. This averaging process is essential for transforming multiple discrete pressure-strain relationships, each valid at a single depth, into a single representative pressure-strain curve that reflects the combined behavior of the entire strain influence zone beneath the footing.

Let ε_j denote a target strain level for which a settlement prediction is desired. For each strain level, ε_j, the PMT pressure P_{ij} is defined as the pressure value extracted from the i^{th} test at that strain level using the three-region logic outlined before. The depth-averaged pressure $\overline{P_j}$ at strain ε_j is then computed using a weighted sum over all test depths provided in Eq. (7).

$$\overline{P_j} = \sum_{i=1}^{n} w_i P_{ij} \tag{7}$$

where: $\overline{P_j}$ is the weighted average pressure at strain level ε_j, P_{ij} is the pressure from test i at strain level ε_j, w_i is the normalized weighted average strain area corresponding to test depth z_i, and n is the total number of PMT tests.

Eq. (7) is evaluated for every strain level in the predefined strain vector $\{\varepsilon_1, \varepsilon_2, \ldots, \varepsilon_m\}$, resulting in a continuous load–settlement curve that accounts for both the stress–strain behavior at each depth and supports the final load–settlement prediction and ensures the settlement response reflects both soil layering and the nonlinear nature of deformation.

3.7. Transformation of PMT Stress-Strain to Footing Load-Settlement Data

The computation of footing settlement in this framework is based on the transformation of PMT strain data into vertical settlement values, using the relationship between soil deformation collected from the pressuremeter and that beneath a shallow foundation. As observed by Briaud (2007), the deformation beneath a spread footing in sand exhibits a barreling pattern similar to the lateral expansion of a cavity in a PMT test. This similarity forms the basis of a method that uses the PMT-derived stress–strain curve to compute the full load-settlement response of a footing.

The method first establishes a relationship between normalized cavity strain and normalized settlement. Specifically, Briaud (2007) proposed the strain equivalence provided in Eq.(8).

$$\frac{s}{B} = 0.24 \cdot \frac{\Delta R}{R_0} \tag{8}$$

where s is the vertical settlement of the footing, B is the footing width, $\Delta R/R_0$ is the normalized radial strain from the PMT test.

Rewriting Eq. (8), the settlement corresponding to any given radial strain level ε_j is computed as:

$$s_j = 0.24 \cdot \varepsilon_j \cdot B, \text{ where } \varepsilon_j = \left(\frac{\Delta R}{R_0} \right) \tag{9}$$

This provides the vertical settlement value s_j at each strain level used in the pressure averaging process described in Section 3.6.

To complete the transformation from PMT data to foundation load–settlement response, the average pressure $\overline{P}_{p,j}$ obtained from PMT tests at strain level ε_j is converted into a corresponding footing pressure $P_{f,j}$. This is done using a transformation factor Γ_j, which accounts for the difference in deformation mode, geometry, and boundary conditions between the two loading conditions. The transformed footing pressure is given in Eq. (10).

$$P_{f,j} = \Gamma_j \cdot \overline{P}_{p,j} \tag{10}$$

The factor Γ_j is not constant but varies with the normalized strain (or settlement) level. Based on a synthesis of experimental load tests and finite element simulations, Briaud and Jeanjean (1994) and Briaud (2007) recommended a conservative design expression for Γ_j as a function of strain, provided in Eq. (11).

$$\Gamma_j = 0.4255 \cdot \left(\frac{\varepsilon_j}{4.2} \right)^{-0.265} \tag{11}$$

This step transforms in-situ radial strain data into a set of footing pressure–settlement pairs ($P_{f,j}$, s_j), forming the core of the predicted load–settlement response. By avoiding empirical moduli and instead using actual stress–strain behavior, the method preserves the nonlinearity and depth sensitivity critical to accurate foundation design.

3.8. Application of Influence Factors and Final Load–Settlement Curve Generation

Before using the pressuremeter-derived load–settlement curve for design, it is essential to account for field-specific conditions that significantly influence how loads are transferred from the foundation to the soil. These include, Fig. 4, the geometry of the footing, the eccentricity and inclination of the applied load, the proximity of the foundation to a slope, and the overall rigidity of the footing system. Each of these factors alters the stress distribution and deformation mechanisms beneath the footing and must therefore be incorporated into the final computed pressures and settlements to ensure design accuracy.

Following the transformation of depth-averaged pressuremeter pressures into equivalent footing pressures using the transfer function Γ_j, as described in Section 3.8, the resulting pressure at a given strain level ε_j is denoted by $P_{f,j.}$ This pressure is further corrected using a composite reduction factor *f*, resulting in a design-adjusted footing pressure given Eq. (12).

$$P_{f,j}^{*} = f \cdot \overline{P}_{p,j} \tag{12}$$

Where $P_{f,j}^{*}$ is the corrected footing pressure that accounts for the composite influence factor *f,* which in turn is the cumulative effects of shape, eccentricity, load inclination, and slope proximity, and is expressed as the product of four individual modifiers provided in Eq. (13).

$$f = f_s \cdot f_e \cdot f_\delta \cdot f_\beta \tag{13}$$

Where each component of *f* is defined below.

The corresponding vertical load applied to the footing at each level is then computed as:

$$Q_j = P_{f,j}^{*} \cdot A = P_{f,j}^{*} \cdot (B \cdot L) \tag{14}$$

These corrected pressure–settlement–load triplets form the final load–settlement curve that reflects both the physical deformation characteristics measured in situ and the boundary and geometric conditions of the actual foundation system. This comprehensive correction framework ensures that the derived response is not only mechanistically accurate but also directly applicable to engineering practice under realistic site constraints.

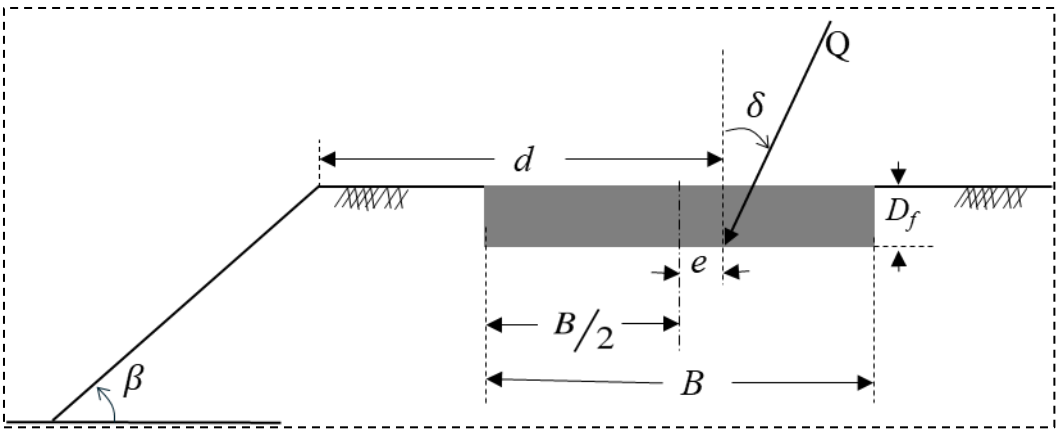

Fig. 4. Shallow foundation influence factors

3.9. Output and Visualization

The final stage of the proposed framework focuses on synthesizing the computed results into interpretable outputs suitable for design evaluation, validation, and documentation. Upon completion of all the processes until the final load-settlement computation, the system generates a series of visualizations and tabular outputs that comprehensively represent the behavior of the soil–foundation system under the applied load.

First, the framework produces detailed plots of the pressure versus radial strain curves for each test depth. These plots include the original measured data, the strain-shifted profiles referenced to the wall contact point, and the extrapolated portion based on the Lemée-type regression model. This visualization offers insight into the deformation behavior across the elastic, plastic, and extrapolated regimes and facilitates qualitative evaluation of the test data quality and the appropriateness of the extrapolation technique. Fig. 5 is a representative strain-stress plot for all depths at a certain borehole with data points shifted to the wall point and the extrapolated portion beyond the loading test data.

Second, a strain influence diagram is generated to illustrate the vertical distribution of strain beneath the foundation based on Schmertmann et al. (1978). This diagram varies depending on the geometry of the footing and is used to validate the calculated influence depths visually, the location of maximum strain, and the extent of the influence zone across different test profiles. Such visualization is particularly valuable for engineers assessing whether sufficient test coverage exists across the active deformation zone.

The stress-strain curves at different depths, Fig. 5, are scaled by the corresponding strain influence area, Fig. 6, and a weighted average pressure is produced, Fig. 7.

A plot of the pressure ratio function Γ as a function of normalized strain ($\Delta R / 4.2R_0$), Fig. 8, is also included. This plot provides an indirect check on the calibration of the transformation from pressuremeter-based pressure to equivalent footing pressure and captures the stiffness degradation pattern with increasing strain. This visual metric supports both design validation and model tuning when compared with independent settlement predictions.

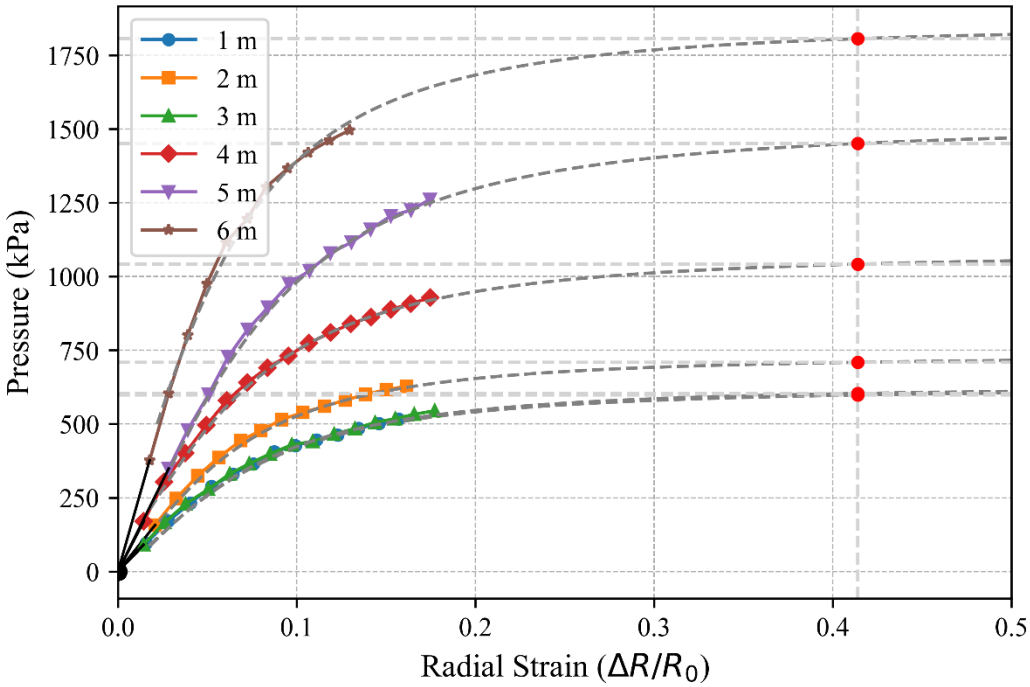

Fig. 5. Stress-strain curves of shifted data points and the Lemée extrapolated portion beyond the maximum loading data points for a sample borehole

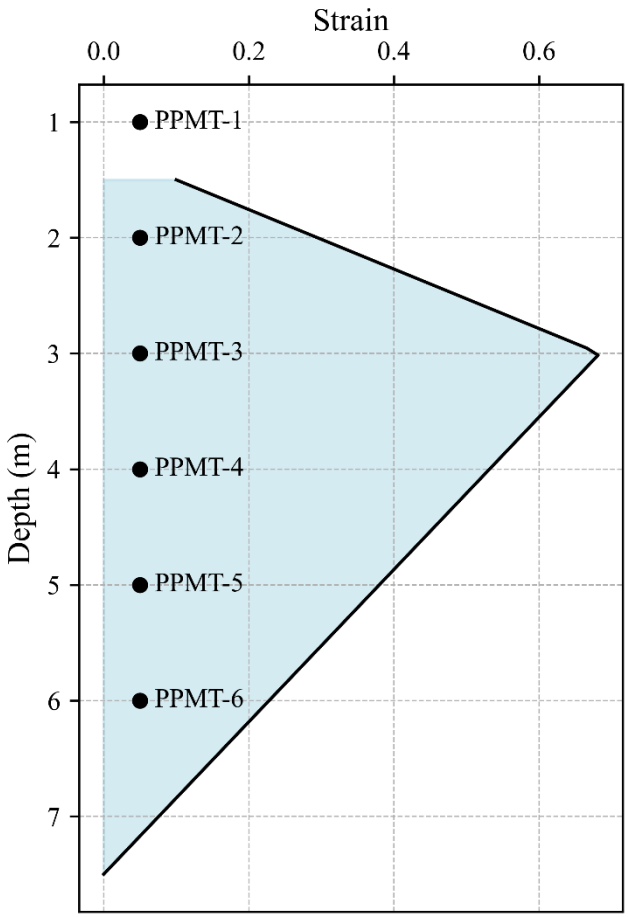

Fig. 6. A sample strain influence factor vs. depth of a square footing placed at 1.5m below the surface, the depths of the PPMT tests are also indicated

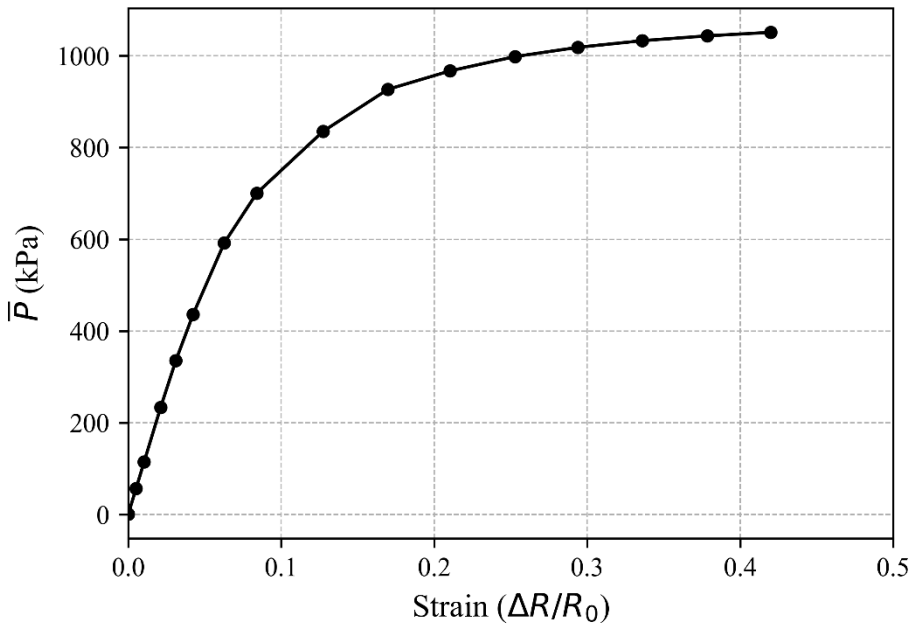

Fig. 7. A weighted average pressure for a sample borehole

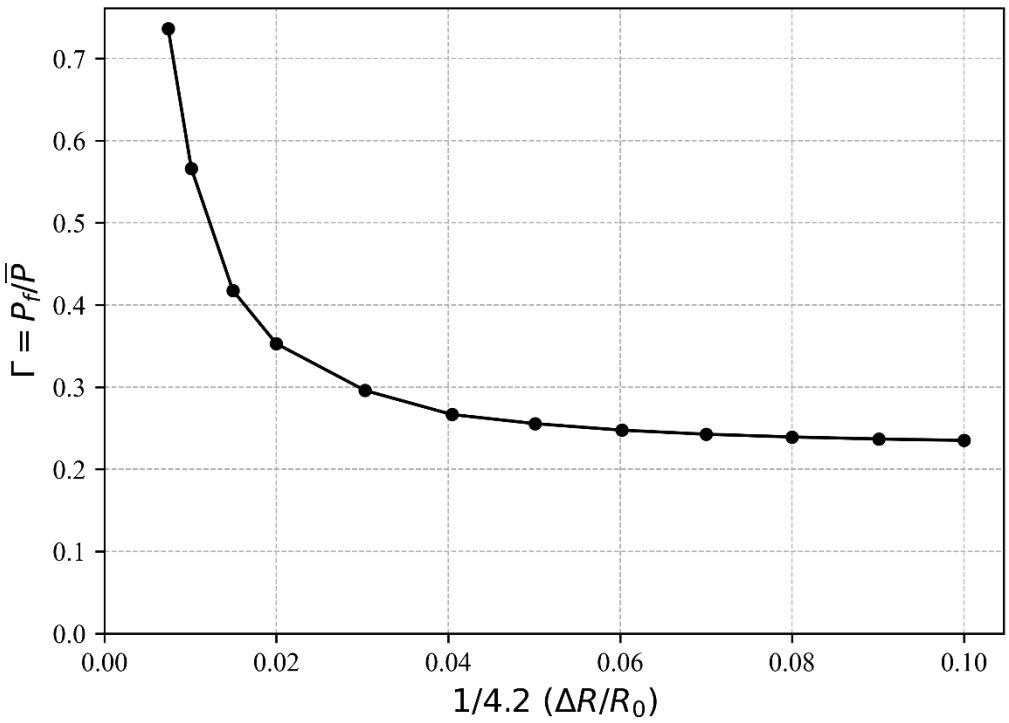

Fig. 8. A normalized stress vs strain curve that used to transform the pressuremeter stress-strain to a load-settlement curve of a shallow footing.

The most critical output is the final load–settlement curve, derived by integrating all correction factors and averaging processes across test depths. This curve directly informs design decisions regarding allowable bearing pressure, estimated settlement under service loads, and potential nonlinearities in the load-displacement response. The curve can be tailored to specific foundation geometries and loading conditions by adjusting the composite influence factors prior to computation, Fig. 9.

To support documentation and further analysis, the system automatically exports all relevant numerical results into structured Excel files. These include a table of pressures extracted at specified strain levels for each test depth, a summary of weighted average pressures across depths, and a comprehensive load-settlement table that incorporates correction factors for shape, eccentricity, inclination, slope proximity. These files serve as both archival datasets and inputs to additional design stages or comparative studies.

All visual outputs are rendered using high-resolution vector graphics, formatted with journal-quality line weights, fonts, and annotations. This ensures that figures are immediately suitable for inclusion in technical reports, academic publications, or presentations without the need for post-processing. By integrating computation, visualization, and data export within a single reproducible pipeline, the framework aligns with the standards of modern geotechnical design and scholarly communication.

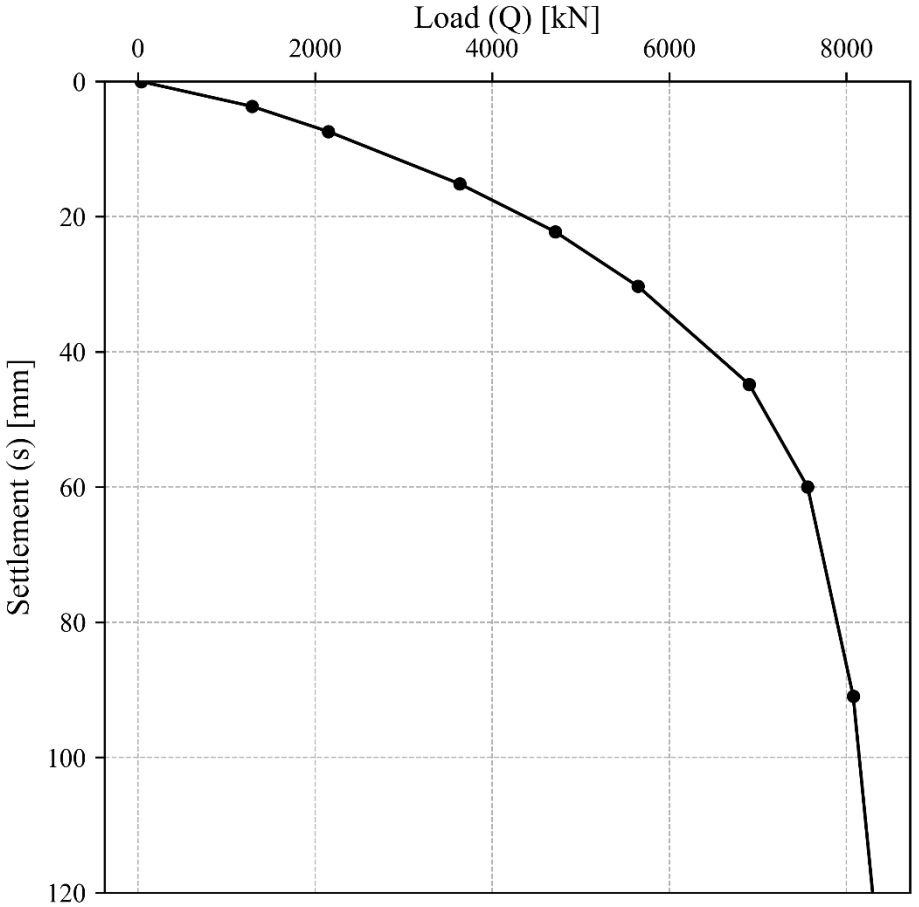

Fig. 9. Load-settlement curve of a sample borehole based on the automated Briaud (2007) approach.

The complete implementation of this automated framework, including sample datasets, annotated scripts, and plotting utilities, is available on GitHub https://github.com/BrhaneWYgzaw/PPMT_Automatic-Load-settlement-curve and has been archived on Zenodo at https://doi.org/10.5281/zenodo.15732472. The automated code implementation used in this study is publicly available Ygzaw (2025).

4. Validation Through Field Case Studies

4.1. Introduction

To demonstrate the effectiveness and practical value of the automated Briaud (2007) framework developed in this study, a series of comparative case studies were conducted using five different in-situ test types across three geotechnically representative sites in Florida. These sites–Kingsley, Trenton, and the University of Central Florida (UCF)–provided diverse, yet well-characterized, sand profiles ideal for evaluating shallow foundation settlement predictions.

For each site, settlement and bearing capacity predictions derived from SPT, CPT, seismic CPT, DMT, and pushed-in PENCEL pressuremeter (PPMT) data were compared. These predictions were benchmarked against full-scale field measurements and finite element simulations using PLAXIS 3D, enabling a robust validation of the automated pressuremeter-based method.

The results show that the PPMT-based approach, implemented using the automated Briaud framework, consistently yields realistic, low-variability settlement curves that fall within accepted serviceability limits. These case studies confirm the framework's applicability across varying soil conditions and reinforce its suitability for geotechnical design in cohesionless sands.

4.2. Site Description and Subsurface Conditions

The three selected field sites represent the dominant geological conditions of Florida's coastal plain, primarily consisting of poorly graded fine sands (USCS SP or SP-SM). Each site was characterized by multiple in-situ tests and borehole logs to establish consistent stratigraphy and soil behavior profiles.

At the Kingsley site, the stratigraphy consisted of loose fine sands extending from the ground surface to a depth of approximately 4 meters. This layer was underlain by medium-dense sand deposits extending to at least 8 meters, with no significant stratigraphic discontinuity. The groundwater table was encountered at approximately 1 meter below the surface, which is typical of shallow phreatic levels in this part of the state.

In contrast, the Trenton site exhibited a thicker surficial layer of loose sands, extending to a depth of approximately 6 meters. Below this, medium-dense sands dominated the profile. The

water table at this location was deeper, recorded at approximately 6 meters, reflecting a localized variation in hydrogeologic conditions relative to the other sites.

The UCF research site presented an inverted soil profile relative to the other locations. Medium-dense sands were observed from the surface to a depth of approximately 5 meters, underlain by looser fine sands extending to about 7 meters. As with the Kingsley site, the water table was encountered near the surface at a depth of approximately 1 meter.

Stratigraphic interpretation at all three sites was supported by grain-size distribution curves and empirical relative density correlations derived from standard penetration test (SPT) blow counts, using the classification guidelines of Terzaghi and Peck (1948). The observed consistency in soil classification and gradation across boreholes at each site enabled meaningful cross-comparison of modulus values derived from different in-situ testing techniques, including pressuremeter, CPT, and SPT.

The geotechnical uniformity within each site, along with controlled testing protocols, provides a reliable basis for evaluating the performance of the proposed settlement prediction framework under conditions representative of cohesionless, granular soils commonly encountered in Florida and other coastal regions.

4.3. Moduli Comparison

This section compares the elastic moduli derived from each test type–SPT, CPT, DMT, TEXAM PMT, and PPMT–across the three sites. Variability, consistency, and methodological influences (e.g., strain level, confinement, test mechanics) are discussed in the context of Fig. 10 and Fig. 11.

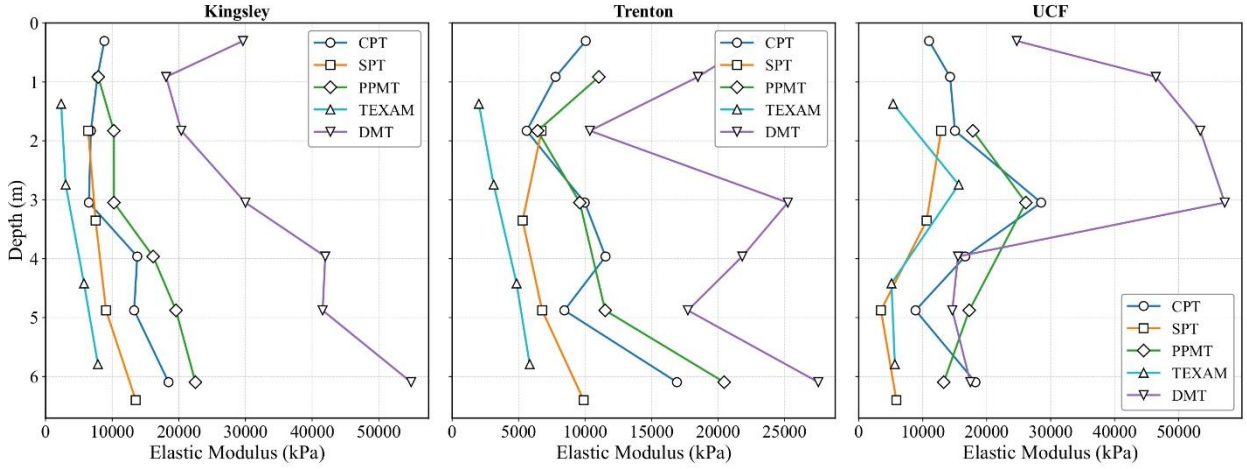

Fig. 10. Modulus profile of the selected in situ tests for the three sites

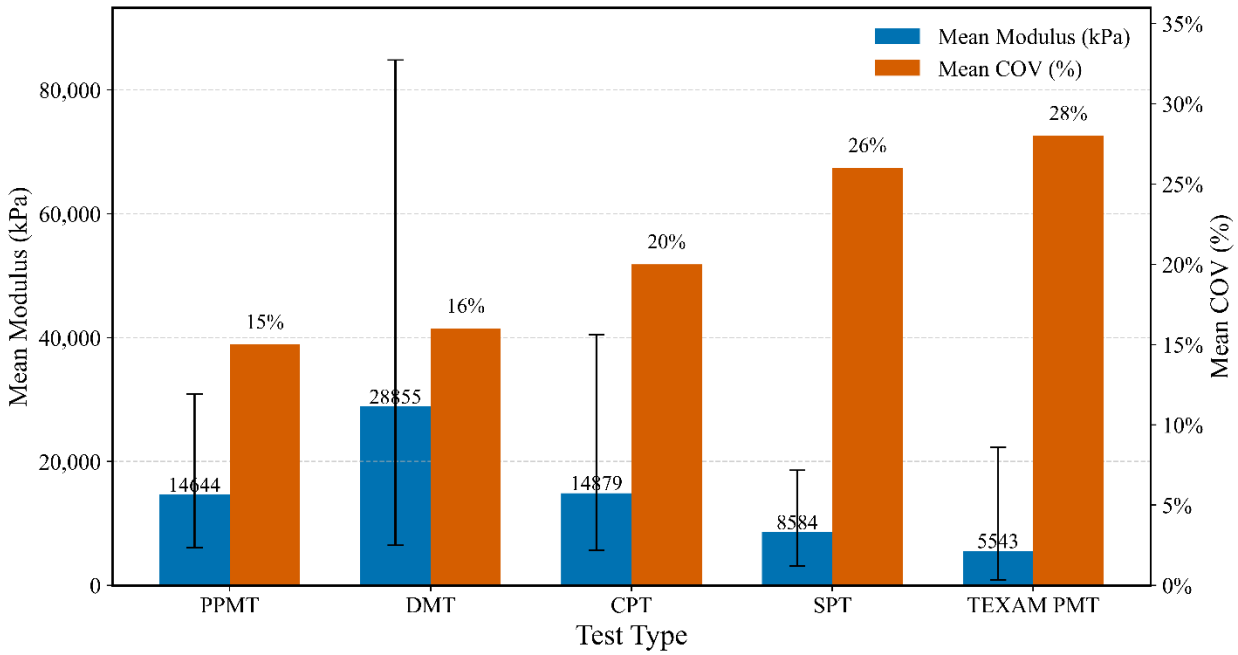

Fig. 11. Average moduli and associated variability across all in-situ test methods.

The SPT modulus was computed based on various methods (Bowles, 1996; Chaplin, 1963; Kulhawy and Mayne, 1990; Sabatini et al., 2002; Webb, 1970). Similar empirical and semi-empirical methods are used to compute the elastic modulus based on CPT data (Buisman, 1940; Beer, 1965; Schmertmann, 1978; Schmertmann, 1970; Thomas, 1968; Webb, 1970). Average moduli of each of the methods considered for the CPT and SPT were considered for the shallow foundation design based on these two in situ tests.

The PPMT and TEXAM PMT modulus values were calculated from pressure–volume expansion or stress-radial strain curves based on elastic modulus formulations of Holtz et al. (1981) and Briaud et al. (1986) approaches, as described in Eq.(15) or Eq. (16). These methods allow for the derivation of moduli at specific strain levels based on cavity expansion theory.

$$E_0 = 2*(1+\upsilon)*\frac{(P_2-P_1)}{(\Delta V_1-\Delta V_2)}*(V_0+0.5*(\Delta V_1+\Delta V_2)) \tag{15}$$

$$E=(1+v)\left[\left(1+\frac{\Delta R_1}{R_o}\right)^2+\left(1+\frac{\Delta R_2}{R_o}\right)^2\right]\frac{\Delta P}{\left(1+\frac{\Delta R_1}{R_o}\right)^2-\left(1+\frac{\Delta R_2}{R_o}\right)^2} \tag{16}$$

The dilatometer modulus (E_D) was calculated using formulations by (Marchetti, 1980) and Marchetti et al. (2006, 2001), Eq. (17). These incorporate lift-off pressure (P_0), limit pressure (P_1), and horizontal stress index (K_D), and induce adjustment based on lateral stress effects.

$$E_D = 34.7\left(P_1 - P_0\right) \tag{17}$$

Error! Reference source not found. presents the elastic modulus profiles derived from five in-situ tests–SPT, CPT, DMT, PPMT, and TEXAM–across the Kingsley, Trenton, and UCF sites in Florida's fine sands. Among these, the DMT generally produced the highest modulus values, particularly at greater depths, owing to its small-strain measurement nature. However, DMT values exhibited considerable variability, potentially reflecting sensitivity to stratigraphic heterogeneity or overestimation at very low strain levels. PPMT and CPT moduli showed a strong correspondence in both magnitude and depth trends despite their methodological differences, with PPMT capturing deformation-controlled stiffness and CPT reflecting penetration resistance. Notably, PPMT tests were conducted using the cone truck typically employed for CPT, which likely contributed to the similar insertion quality and consistent profiling. SPT moduli, derived empirically from N-values, ranked low and were highly variable, underscoring the limitations of using failure-based penetration resistance to infer stiffness. TEXAM PMT consistently yielded the lowest modulus values at all sites, a result linked to the disturbance from open borehole preparation using SPT drilling rigs. The loss of confinement and potential relaxation of soil during borehole preparation likely reduced the soil's measured stiffness. These findings highlight the importance of both the probe insertion methods and test mechanics when interpreting modulus profiles for settlement or stiffness-based foundation design

4.4. Settlement and Bearing Capacity

Predicted settlements from five in-situ test methods are compared for a shallow foundation representative of typical low-rise structures. A 3 m × 3 m footing under a 2200 kN load was used as the reference case for evaluating deformation behavior and bearing resistance. Settlement predictions are examined against serviceability thresholds, and bearing capacities are assessed across empirical, theoretical, and pressuremeter-based methods. The results underscore the reliability of the automated Briaud method using PPMT data.

Fig. 12 reflects the predicted settlements for this footing configuration. Among the five in-situ test methods evaluated–SPT, CPT, PPMT, TEXAM pressuremeter, and DMT–the SPT-based method, (Anagnostopoulos et al., 1991; Bowles, 1987; Burland et al., 1985; Meyerhof, 1965; Parry, 1985; Peck et al., 1974; Peck and Bazaara, 1969; Poulos and Davis, 1974; Schleicher, 1926; Teng, 1962; Terzaghi and Peck, 1968; Tschebotarioff, 1973; Webb, 1970), consistently produced the highest settlement predictions across all sites, often exceeding ≈59 mm, with substantial variability, particularly at the Trenton and UCF locations. CPT, (Bowles, 1987; De Beer and Martens, 1957; De Beer, 1965; Meyerhof, 1965; Poulos and Davis, 1974; Schleicher, 1926; J. H. Schmertmann, 1978; Tschebotarioff, 1973), estimates were moderately lower and showed improved consistency. TEXAM pressuremeter results (Briaud, 2007; Ménard, 1967) generally fell between penetration-based and displacement-based methods, with relatively uniform predictions. Both PPMT (Briaud, 2007; Ménard, 1967) and DMT (Leonards and Frost, 1988; Schmertmann, 1986) yielded settlements below the commonly accepted tolerable limit of 25 mm; however, while DMT often predicted the lowest mean values, its results exhibited greater variability and were not consistently smaller than those from PPMT. Overall, displacement-based methods (PPMT and

DMT) produced lower and more consistent settlement estimates within the serviceability threshold.

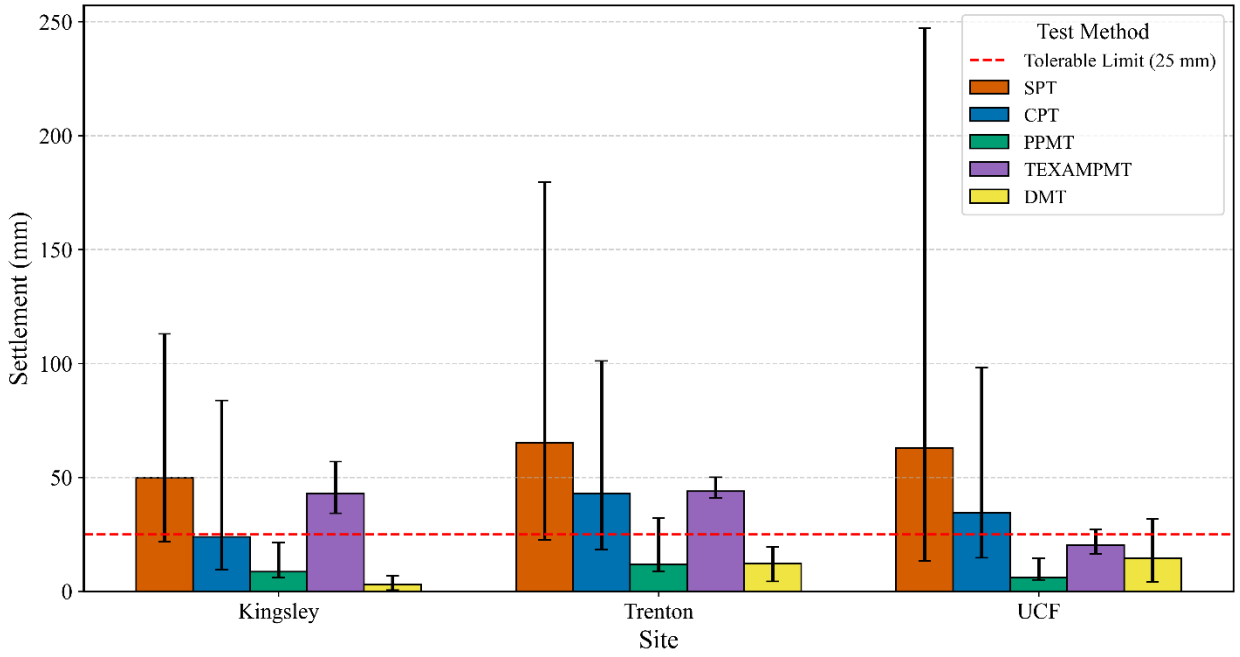

Fig. 12. Predicted average settlements from five in-situ tests at three sites for a 3 m × 3 m foundation under a 2200 kN (500 kips) load. Error bars show min–max range; red line indicates 25 mm tolerable limit.

The comparative analysis of average bearing capacities derived from diverse in-situ test methods reveals distinct trends across test categories and sites, Fig. 13. SPT-based approaches (Bowles, 1996; Meyerhof, 1956; Parry, 1977; Teng, 1962), consistently yield the lowest and most conservative estimates, typically below 700 kPa, and exhibit significant variability due to their empirical nature and sensitivity to field conditions. In contrast, CPT-based methods, (Meyerhof, 1956; John H. Schmertmann, 1978), produce the highest values, often exceeding 6000 kPa, indicating potential overestimation when uncalibrated for local soil conditions.

PMT-based methods (Briaud, 1992; Ménard and Rousseau, 1962), particularly results-based PPMT data, provide intermediate and more consistent results, aligning closely with the adjusted average bearing capacity (approximately 1070 kPa), thereby supporting their reliability in practical design applications. However, results based on TEXAM PMT data are still below the average value when all approaches are considered. Theoretical methods (Beer, 1970; Hanna and Meyerhof, 1981; Hansen, 1970; Meyerhof, 1963; Terzaghi, 1943; Vesić, 1973) show moderate and relatively uniform predictions across all sites, making them useful as baseline estimators.

Despite the broad spread in predictions, the combined results suggest that a bearing capacity range of approximately 900–1100 kPa is reasonable for shallow foundations on similar fine sands. The alignment of the PPMT data-based prediction with this representative range reinforces its applicability for both routine engineering practice and geotechnical research.

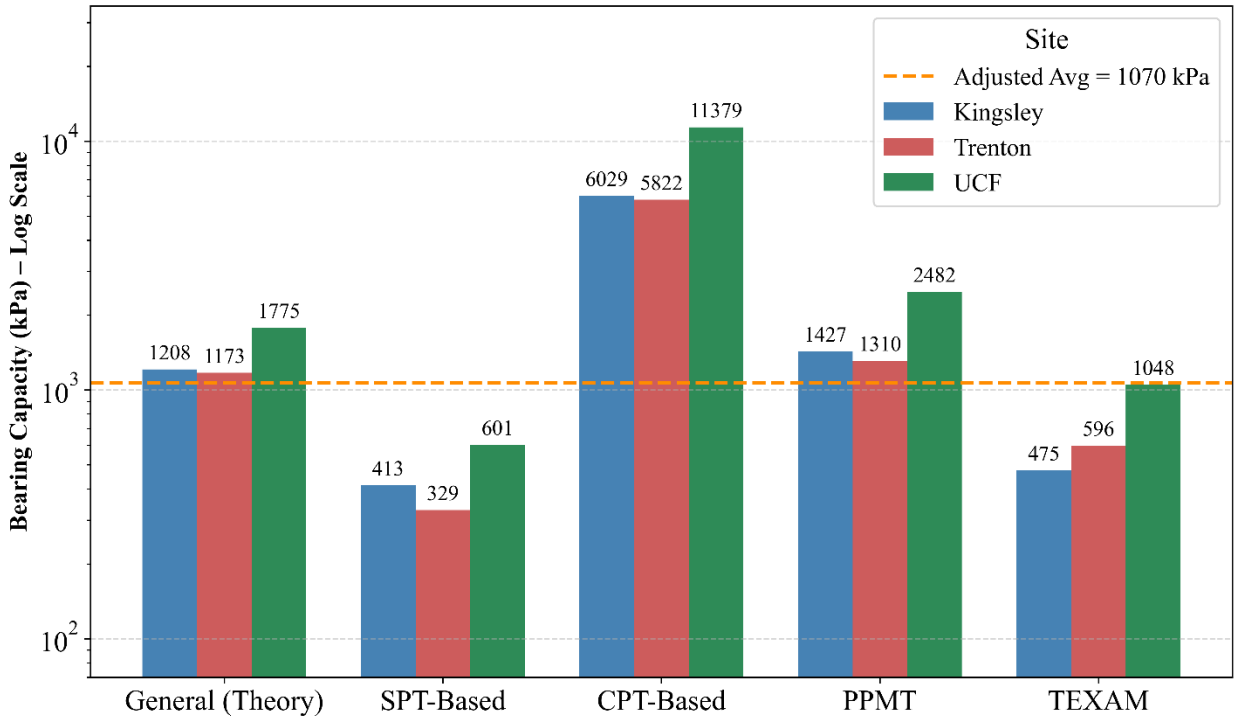

Fig. 13. Comparison of average bearing capacity (in kPa, log scale) computed from various in-situ test methods across three Florida sites (Kingsley, Trenton, and UCF).

The PPMT data-based settlement and bearing capacity are more consistent near the average value, considering all approaches respectively. Moreover, the Briaud (2007) approach, which comprehensively provides settlement and bearing capacity, has more advantages over the other methods. In the next portion of this study, this method was compared and validated with numerical simulations based on traditional and advanced soil models as well as full-scale measured data.

4.5. Comparison of Briaud (2007) and Numerical Approach

Traditional analytical methods often rely on simplified assumptions and may not accurately capture the complex behavior of soil under an applied load. Numerical methods like the finite element method (FEM) offer a more detailed and accurate approach to predicting settlements by modeling the soil-structure interaction with higher fidelity.

FEM lets engineers simulate shallow foundation behavior with realistic soil properties, including nonlinear stress-strain relationships, anisotropy, and heterogeneity. It models complex foundation geometries and load conditions, like eccentric or inclined loads. FEM also considers factors such as soil layering, consolidation, and groundwater conditions, offering a thorough settlement assessment.

In contrast, numerical methods, particularly advanced models, require various parameters to accurately simulate geotechnical phenomena. This study employs the traditional Mohr-Coulomb (MC) model as well as two advanced models, the hardening soil (HS) and hardening

soil-small (HSS) models, for the numerical analysis of a representative shallow foundation at three field sites.

4.5.1. Calibration of Model Parameters

The values of the parameters of the three models are commonly chosen using Triaxial test data. However, these sites have insufficient triaxial test data to calibrate the three models' parameters. The parameters of the three models can be correlated with various in situ test values from SPT, CPT, and DMT (Ygzaw, 2025). As a result, data from the CPT testing were used to calibrate the parameters of the three models. Correlations of the models' parameters with relative density (D_r) consistently fall within expected ranges for soils at the three sites. Table 2 summarizes the parameter correlations with D_r as adopted from Brinkgreve et al. (2010). Moreover, Table 3 presents the soil parameters for the three sites, required by each numerical model.

Table 2. Calibration of Model Parameters

Parameter	Calibrated from	Approach/Methodology	Numerical Model	Unit
E_{50}^{ref}	CPT	1253*Dr	HS, and HS small	kPa
E_{oed}^{ref}	CPT	1253*Dr	HS, and HS small	kPa
E_{ur}^{ref}	CPT	3759.4*Dr	HS, and HS small	kPa
G_0^{ref}	CPT	1253+1420*Dr	HS small	kPa
$\gamma_{0.7}$	CPT	$(2 - D_r) * 10^{-4}$	HS small	[-]
m	CPT	$0.7 - {D_r}/{320}$	HS small	*
j'	CPT and SPT	$28 + 12.5 * D_r$	HS small	[0]
y	CPT	$-2 + 12.5 * D_r$ or j-30	HS small	[0]
R_f	CPT	$1 - {D_r}/{800}$	HS small	*

*Dr is in percentage

Table 3. Numerical model parameters for the three field sites

Parameter	Unit	Kingsley site		Trenton site		UCF site	
		Layer 1	Layer 2	Layer 1	Layer 2	Layer 1	Layer 2
g unsaturated	kN/m^3	17.7	18.4	17.7	18.4	17.7	18.4
g saturated	kN/m^3	18.8	19.5	18.8	19.5	18.8	19.5
j	[^{0}]	29	34	29	32	31.4	29.83
y	[^{0}]	0	4	0	2	0	0

E_{ref}	kPa	26142	36676	25951	26669	34809	27627
E_{50}^{ref}	kPa	26142	36676	25951	26669	34809	27627
E_{oed}^{ref}	kPa	26142	36676	25951	26669	34809	27627
E_{ur}^{ref}	kPa	78523	110316	78092	80055	104283	82976
G_0^{ref}	kPa	88722	103660	89488	90254	98872	96765
$\gamma_{0.7}$	[-]	$1.58*10^{-4}$	$1.36*10^{-4}$	$1.57*10^{-4}$	$1.55*10^{-4}$	$1.45*10^{-4}$	$1.47*10^{-4}$
m	[-]	0.5	0.5	0.5	0.5	0.5	0.5
v_{ur}	[-]	0.2	0.2	0.2	0.2	0.2	0.2
p^{ref}	kPa	100	100	100	100	100	100
K_0^{nc}	[-]	0.5152	0.4408	0.5152	0.5152	0.4408	0.5152
R_f	[-]	0.9	0.9	0.9	0.9	0.9	0.9

4.5.2. PLAXIS-3D Model Geometry

A finite element method (FEM) analysis was conducted using a Plaxis3D model of dimensions 30 m by 30 m with a depth of 6 m. This model aimed to minimize boundary effects on settlement predictions for a square footing measuring 3 m by 3 m. The model depth is fixed at 6 m, considering a 2B depth of influence of the square footing. Models with vertical boundaries at 10 m depth were also tested and showed minimal impact on predicted settlement.

The 3 m by 3 m concrete footing, placed at a depth of 1.5m from the surface, was represented as a rigid plate in the model. Table 4 illustrates the properties of the horizontal and vertical plates used for the footing and retaining walls, which support the vertically cut soil during foundation construction.

Table 4. Parameters for the foundation plates

Parameter	Floor plate	Wall plate	Unit
Unit weight, γ	146	146	Kip/f3
Isotropic	yes	yes	
Young's modulus, E1	$626.4*10^6$	$626.4*10^6$	Kip/f^2
Shear modulus, G	$272.35*10^6$	$272.35*10^6$	Kip/f^2
Poisson's ratio	0.15	0.15	[]
Thickness	3	3	ft

4.5.3. Numerical Analysis Results

The load-settlement results of the various numerical simulation models were summarized and compared with the results of Briaud (2007). As elaborated in the previous section, to avoid

any bias, the parameters of all the models were calibrated from relative density, which was in turn calculated from the CPT test.

The load-settlement results of the three sites based on numerical simulation and Briaud (2007) are shown in Figs. 14-16. The HS and HSS models align with Briaud (2007), but the MC model, which is based on an elastic-perfect plastic model, predicts higher settlements due to its simplified nature and insufficient stiffness parameters for cohesionless soils.

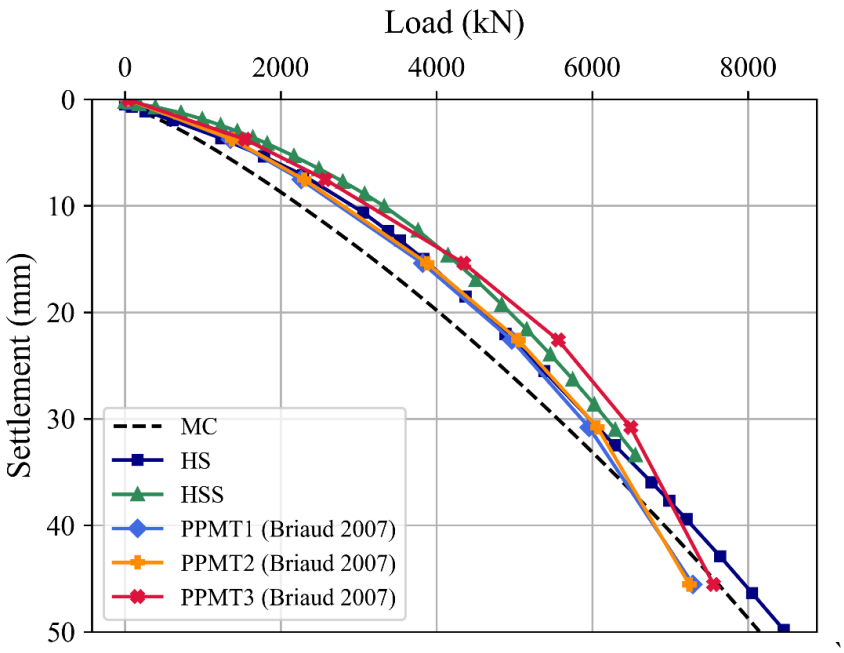

Fig. 14. Load-Settlement prediction based on Briaud (2007) and Numerical simulations at the Kingsley site

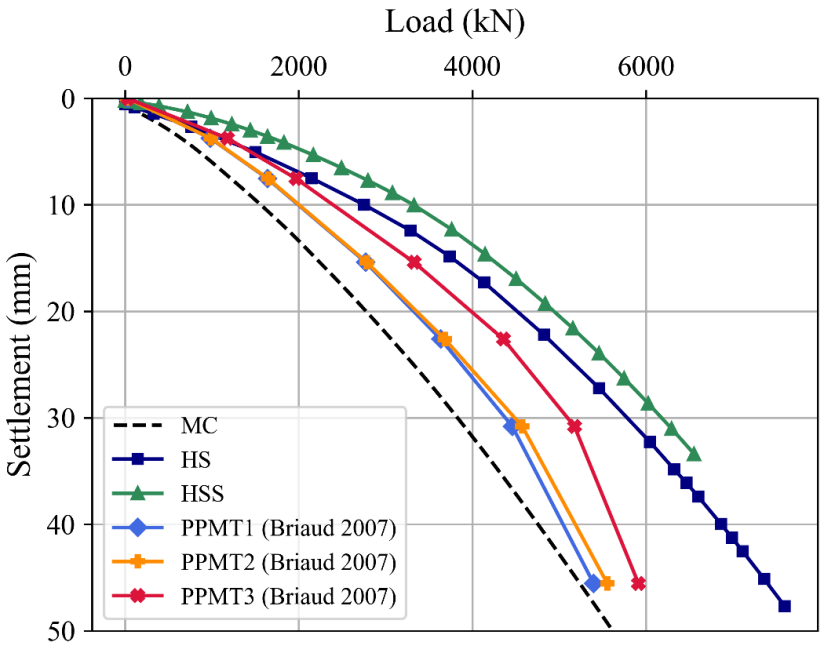

Fig. 15. Load-Settlement prediction based on Briaud (2007) and Numerical simulations at Trenton

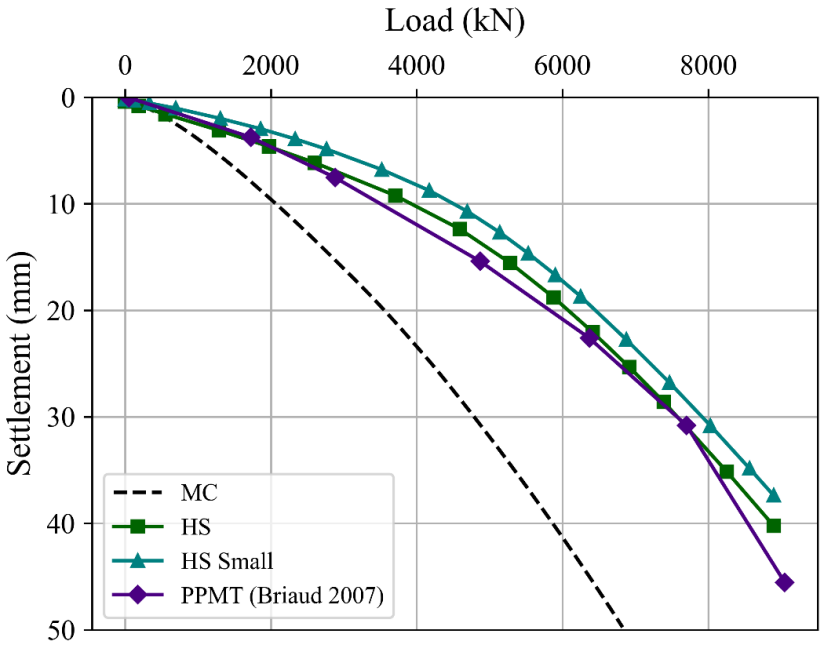

Fig. 16. Load-Settlement prediction based on Briaud (2007) and Numerical simulations at UCF

4.5.4. Comparison of Briaud (2007) with Measured and Simulated Load-Settlement Results at the UCF Site

Field measurements from conical loading experiments at the UCF research site are used to benchmark the predicted settlement curves from both the Briaud method and numerical models. Agreement across all approaches further supports the practical applicability of the proposed framework.

For the three field sites, although a series of plate load tests were conducted, a maximum load of 20 kN was applied on a 0.3 m diameter plate. This was not sufficient to produce the load and corresponding settlement that a common shallow foundation footing produces.

One potential comparison of predicted and measured settlements was made for the UCF site. This site is the UCF research site where three conically loaded areas were placed at the surface to enable settlements to be measured (Chopra and Arboleda-Monsalve, 2020).

A conical soil mound, 4 m high and 12 m in diameter, which forms an angle of repose of approximately 35 °, was used by the UCF as an applied load. The soil cone was loosely dumped, producing a unit weight of 15.7 kN/m^3. A magnetic extensometer (spider magnet), datum magnet (placed around 14 m depth), displacement transducer, and surveying equipment were used to measure the settlement due to the conical loading. Pressure cells were also used to measure the pressure of the conical surcharge. Details of the arrangement are given in Chopra and Arboleda-Monsalve (2020). Fig. 17 summarizes the comparison of the measured and predicted load-settlement curves at the UCF site.

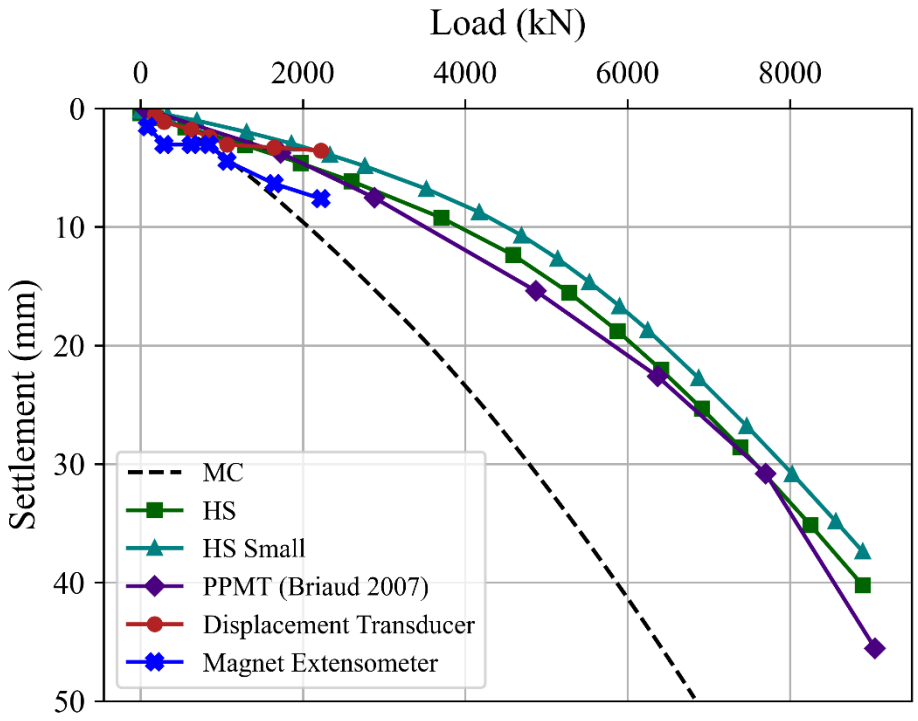

Fig. 17. Comparison of measured and predicted load-settlements

Though it is still hard to produce a bigger reaction load, the load-settlement curves from the three approaches, the Briaud (2007) prediction, the numerical simulations, and the measured data based on the two instruments are well fitted up to the load-settlement level that the conical soil mound can produce.

5.Discussion

The development of a fully automated Python-based implementation of Briaud's pressuremeter settlement method (Briaud, 2007) represents a practical advancement in deformation-based foundation design, particularly in cohesionless soils where empirical methods often struggle to capture true soil behavior. By deriving settlement directly from in-situ stress–strain data captured by the PPMT, the framework preserves the nonlinear, depth-dependent nature of soil response, without relying on assumed moduli or empirical fitting.

Across all three study sites, the PPMT-based approach outperformed traditional in-situ test methods (SPT, CPT, DMT, and TEXAM PMT) in terms of both consistency and realism. Notably, the predicted settlements from the PPMT data aligned closely with those obtained from full-scale field measurements and advanced numerical simulations, particularly the Hardening Soil and HS-small models. The use of pushed-in PENCEL pressuremeter data proved advantageous over pre-bored TEXAM tests, likely due to reduced disturbance and better confinement. This is especially relevant in sandy soils, where subtle changes in stiffness can significantly affect settlement predictions.

The proposed framework also demonstrated close agreement with measured field settlements under a conical soil mound at the UCF research site, reinforcing its validity in real-world applications. While the DMT provided similar magnitude predictions, its variability across depth limited its reliability compared to the more stable PPMT-based estimates. SPT and CPT methods, although widely used, showed larger variability and, in some cases, overpredicted settlement, highlighting the limitations of penetration resistance as a proxy for deformation behavior.

While high-quality pressuremeter data remains essential for optimal results, the framework's built-in extrapolation techniques and standardized analysis steps help mitigate common field challenges such as curve truncation or insertion effects. The method's successful application across three varied Florida sites demonstrates its robustness in cohesionless soils and suggests strong potential for integration into routine geotechnical design practice.

6. Conclusion

This study introduced a Python-based automated framework for predicting shallow foundation settlements using Briaud's (2007) method, adapted for pushed-in PENCEL Pressuremeter (PPMT) data. The following key conclusions can be drawn:

1. *Automation of Briaud's Method*: The framework successfully automates all major steps of Briaud's procedure, including wall-point detection, Lemée-type curve extrapolation, strain

influence zoning, and correction factor integration, making a previously manual process reproducible and accessible.

2. *Effective Use of PPMT Data*: Adaptation to pushed-in PENCEL pressuremeter data allows for reduced soil disturbance and high-resolution stiffness profiling in cohesionless soils. The method addresses common field limitations such as incomplete pressuremeter curves.
3. *Validation through Field and Numerical Studies*: Predicted settlements showed strong agreement with results from advanced PLAXIS 3D simulations (MC, HS, and HS-small models) and full-scale field measurements, particularly at the UCF site. This confirms the reliability of the automated method in sandy soils.
4. *Superior Performance over Traditional Methods*: Compared to other in-situ tests (SPT, CPT, DMT, and TEXAM PMT), the PPMT-based framework produced more consistent and physically realistic settlement estimates, staying within acceptable serviceability limits.
5. *Open-Source and Scalable*: By offering an open-source implementation, the framework supports transparency, reproducibility, and broader adoption. It is modular and adaptable for integration with modern digital workflows in geotechnical design.
6. *Future Applicability*: While this study focused on uniform granular soils, the framework provides a foundation for future extensions to layered or mixed profiles. With additional tools, such as digital borehole integration or machine learning, it may be applied across a wider range of site conditions.

Acknowledgement

The authors gratefully acknowledge the financial support provided by the Florida Department of Transportation (FDOT) under Grant No. BED28 977-01. This support was essential to the successful completion of the research presented in this paper.

References

Anagnostopoulos, A.G., Papadopoulos, B.P., Kavvadas, M.J., 1991. Direct estimation of settlements on sand, based on SPT results.

Aouadj, A., Bouafia, A., 2022. CPT-based method using hybrid artificial neural network and mathematical model to predict the load-settlement behaviour of shallow foundations. Geomechanics and Geoengineering 17, 321–333. https://doi.org/10.1080/17486025.2020.1755459

Bagińska, M., Srokosz, P.E., 2019. The optimal ANN Model for predicting bearing capacity of shallow foundations trained on scarce data, KSCE Journal of Civil Engineering. Elsevier.

Baguelin, F., Jézéquel, J.F., Shields, D.H., 1978. The Pressuremeter and Foundation Engineering. Trans Tech Publications.

Bowles, J.E., 1996. Foundation analysis and design, 5. ed., internat. ed. ed. McGraw-Hill, New York.

Bowles, J.E., 1987. Elastic Foundation Settlements on Sand Deposits. J. Geotech. Engrg. 113, 846–860. https://doi.org/10.1061/(ASCE)0733-9410(1987)113:8(846)

Briaud, J.-L., 2007. Spread Footings in Sand: Load Settlement Curve Approach. J. Geotech. Geoenviron. Eng. 133, 905–920. https://doi.org/10.1061/(ASCE)1090-0241(2007)133:8(905)
Briaud, J.-L., 1992. The Pressuremeter. Routledge, London. https://doi.org/10.1201/9780203736173
Briaud, J.-L., Jeanjean, P., 1994. Load settlement curve method for spread footings of sand, in: Vertical and Horizontal Deformations of Foundations and Embankments. ASCE, pp. 1774–1804.
Briaud, J.L., Terry, T.A., Cosentino, P.J., Tucker, L.M., Lytton, R.L., 1986. Influence of Stress, Strain, Creep and Cycles on Moduli from Preboring and Driven Pressuremeters. Department of Civil Engineering, Rep. No. RF-7035, Texas A&M University, College Station, TX.
Brinkgreve, R.B.J., Engin, E., Engin, H.K., 2010. Validation of empirical formulas to derive model parameters for sands. Numerical methods in geotechnical engineering 137, 142.
Buisman, A. S. K., 1940. Groundmechania.
Burland, J., Burbidge, M., Wilson, E., TERZAGHI, 1985. SETTLEMENT OF FOUNDATIONS ON SAND AND GRAVEL. Proceedings of the Institution of Civil Engineers 78, 1325–1381. https://doi.org/10.1680/iicep.1985.1058
Chaplin, T.K., 1963. The compressibility of granular soils, with some applications to foundation engineering, in: Proceedings of the 2nd European Conference on Soil Mechanics and Foundation Enigneering, Wiesbaden. pp. 215–219.
Chopra, M., Arboleda-Monsalve, L.G., 2020. Comparison of Standard Penetration Test (SPT) N-value with Alternative Field Test Methods in Determining Moduli for Settlement Predictions.
De Beer, E., Martens, A., 1957. Method of computation of an upper limit for the influence of heterogeneity of sand layers in the settlement of bridges, in: Proceedings, 4th International Conference on Soil Mechanics and Foundation Engineering, London. pp. 275–281.
De Beer, E.E., 1970. Experimental Determination of the Shape Factors and the Bearing Capacity Factors of Sand. Géotechnique 20, 387–411. https://doi.org/10.1680/geot.1970.20.4.387
De Beer, E.E., 1965. Bearing capacity and settlement of shallow foundations on sand, in: Proc. Symp. Bearing Capacity and Settlement of Foundations. Duke University, pp. 15–34.
Hanna, A.M., Meyerhof, G.G., 1981. Experimental evaluation of bearing capacity of footings subjected to inclined loads. Can. Geotech. J. 18, 599–603. https://doi.org/10.1139/t81-072
Hansen, J.B., 1970. A revised and extended formula for bearing capacity.
Holtz, R.D., Kovacs, W.D., Sheahan, T.C., 1981. An introduction to geotechnical engineering. Prentice-hall Englewood Cliffs, NJ.
Hough, B.K., 1959. Compressibility as the Basis for Soil Bearing Value. J. Soil Mech. and Found. Div. 85, 11–40. https://doi.org/10.1061/JSFEAQ.0000207
Jin, Y.-F., Yin, Z.-Y., Zhou, W.-H., Horpibulsuk, S., 2019. Identifying parameters of advanced soil models using an enhanced transitional Markov chain Monte Carlo method, Acta Geotechnica. Springer.
Kulhawy, F.H., Mayne, P.W., 1990. Manual on estimating soil properties for foundation design. Electric Power Research Inst., Palo Alto, CA (USA); Cornell Univ., Ithaca ….

LEMÉE, E., 1973. Simulation analytique de la courbe pressiométrique (Internal Document (Not Published)). Laboratoire Régional des Ponts et Chaussées de Saint-Brieuc, Saint-Brieuc, France.
Leonards, G.A., Frost, J.D., 1988. Settlement of Shallow Foundations on Granular Soils. J. Geotech. Engrg. 114, 791–809. https://doi.org/10.1061/(ASCE)0733-9410(1988)114:7(791)
Liu, Y., Liang, Y., 2024. Integrated machine learning for modeling bearing capacity of shallow foundations, Scientific Reports. Nature Publishing Group UK London.
Marchetti, S., 1980. In Situ Tests by Flat Dilatometer. J. Geotech. Engrg. Div. 106, 299–321. https://doi.org/10.1061/AJGEB6.0000934
Marchetti, S., Monaco, P., Calabrese, M., Totani, G., 2006. Comparison of moduli determined by DMT and backfigured from local strain measurements under a 40 m diameter circular test load in the Venice area, in: Proc. 2nd Int. Conf. on the Flat Dilatometer, Washington DC. pp. 220–230.
Marchetti, S., Monaco, P., Totani, G., Calabrese, M., 2001. The flat dilatometer test (DMT) in soil investigations–A report by the ISSMGE committee TC16. Proc. In Situ 41.
Marto, A., Hajihassani, M., Momeni, E., 2014. Bearing capacity of shallow foundation's prediction through hybrid artificial neural networks. Applied mechanics and materials 567, 681–686.
Mayne, P.W., Poulos, H.G., 1999. Approximate Displacement Influence Factors for Elastic Shallow Foundations. J. Geotech. Geoenviron. Eng. 125, 453–460. https://doi.org/10.1061/(ASCE)1090-0241(1999)125:6(453)
Ménard, L., 1967. Règles d'utilisation des techniques pressiométriques et d'exploitation des résultats obtenus pour le calcul des fondations. Notice générale D 60.
Ménard, L., Rousseau, J., 1962. L'évaluation des tassements, tendances nouvelles. Sols Soils 1, 13–29.
Meyerhof, G.G., 1965. Shallow Foundations. J. Soil Mech. and Found. Div. 91, 21–31. https://doi.org/10.1061/JSFEAQ.0000719
Meyerhof, G.G., 1963. Some Recent Research on the Bearing Capacity of Foundations. Can. Geotech. J. 1, 16–26. https://doi.org/10.1139/t63-003
Meyerhof, G.G., 1956. Penetration Tests and Bearing Capacity of Cohesionless Soils. J. Soil Mech. and Found. Div. 82. https://doi.org/10.1061/JSFEAQ.0000001
Mohanty, R., Das, S.K., 2018. Settlement of shallow foundations on cohesionless soils based on SPT value using multi-objective feature selection, Geotechnical and Geological Engineering. Springer.
Oweis, I.S., 1979. Equivalent Linear Model for Predicting Settlements of Sand Bases. J. Geotech. Engrg. Div. 105, 1525–1544. https://doi.org/10.1061/AJGEB6.0000904
Papadopoulos, B.P., 1992. Settlements of Shallow Foundations on cohesionless soils. J. Geotech. Engrg. 118, 377–393. https://doi.org/10.1061/(ASCE)0733-9410(1992)118:3(377)
Parry, R.H.G., 1985. A direct method of estimating settlements in sand from SPT values, in: Golden Jubilee of the International Society for Soil Mechanics and Foundation Engineering: Commemorative Volume. Institution of Engineers, Australia Barton, ACT, pp. 166–174.
Parry, R.H.G., 1977. Estimating Bearing Capacity in Sand from SPT Values. J. Geotech. Engrg. Div. 103, 1014–1019. https://doi.org/10.1061/AJGEB6.0000484

Peck, R.B., Bazaara, A.R.S., 1969. Settlement of spread footings on sand: Discussion of the paper by D'Appolonia et al. Journal of Soil Mechanics and Foundation Division, ASCE 95.
Peck, R.B., Hanson, W.E., Thornburn, T.H., 1974. Foundation Engineering.‖ John Wiley & Sons. Inc, New York.
Poulos, H.G., Davis, E.H., 1974. Elastic solutions for soil and rock mechanics. (No Title).
Sabatini, P.J., Bachus, R.C., Mayne, P.W., Schneider, J.A., Zettler, T.E., GeoSyntec Consultants, 2002. Geotechnical Engineering Circular No. 5 Evaluation of Soil and Rock Properties (No. FHWA-IF-02-034).
Schleicher, F., 1926. Zur theorie des baugrundes. Bauingenieur 48, 931–935.
Schmertmann, J.H., 1986. Dilatometer to compute foundation settlement. Use of insitu tests in geotechnical engineering, Geotechnical Special Publication 303–321.
Schmertmann, J. H., 1978. Measurement of insitu shear strength: Proc Conference on In-situ Measurement of Soil Properties, Raleigh, NC, 1–4 June 1975, V2, P57–138, disc P139–179, in: International Journal of Rock Mechanics and Mining Sciences & Geomechanics Abstracts. Pergamon, p. 67.
Schmertmann, John H., 1978. Guidelines for cone penetration test : performance and design (No. FHWA-TS-78-209).
Schmertmann, J.H., 1970. Static Cone to Compute Static Settlement Over Sand. J. Soil Mech. and Found. Div. 96, 1011–1043. https://doi.org/10.1061/JSFEAQ.0001418
Schmertmann, J.H., Hartman, J.P., Brown, P.R., 1978. Improved Strain Influence Factor Diagrams. J. Geotech. Engrg. Div. 104, 1131–1135. https://doi.org/10.1061/AJGEB6.0000683
Teng, W.C., 1962. Foundation Design. Prentice-Hall, Inc.
Terzaghi, K., 1943. Theoretical soil mechanics.
Terzaghi, K., Peck, R.B., 1968. Soil Mechanics in Engineering Practice: Second (2nd) Edition, Second Edition. ed. John Wiley & Sons.
Terzaghi, K., Peck, R.B., 1948. Soil mechanics in engineering practice. John wiley & sons.
Thomas, D., 1968. Deepsounding Test Results and the Settlement of Spread Footing on Normally Consolidated Sands. Géotechnique 18, 472–488. https://doi.org/10.1680/geot.1968.18.4.472
Tschebotarioff, G.P., 1973. Foundations, Retaining and Earth Structures: The Art of Design and Construction and Its Scientific Basis in Soil Mechanics, 2nd edition. ed. McGraw-Hill, New York.
Vesić, A.S., 1973. Analysis of Ultimate Loads of Shallow Foundations. J. Soil Mech. and Found. Div. 99, 45–73. https://doi.org/10.1061/JSFEAQ.0001846
Webb, D.L., 1970. SETTLEMENT OF STRUCTURES ON DEEP ALLUVIAL SANDY SEDIMENTS IN DURBAN, SOUTH AFRICA.
Ygzaw, B. W., 2025. PPMT Automated Load–Settlement Prediction Framework.
Ygzaw, B.W., 2025. Use of Pushed-in PENCEL Pressuremeter Test for Shallow Foundation Design in Florida Fine Sands (Doctoral dissertation). Florida Institute of Technology, Melbourne, FL, USA.